Int. J. Solids Structures Vol. 30, No. 2, pp. 273–286, 1993
Printed in Great Britain.

0020-7683/93 $5.00+.00

SENSITIVITY OF THE RESPONSE OF MODERATELY THICK CROSS-PLY DOUBLY-CURVED PANELS TO LAMINATION AND BOUNDARY CONSTRAINT—II. APPLICATION

REAZ A. CHAUDHURI and HUMAYUN R. H. KABIR†
Department of Civil Engineering, University of Utah, 3220 Merrill Engineering Buildings, Salt Lake City, UT 84112, U.S.A.

(*Received* 26 *February* 1991; *in revised form* 10 *June* 1992)

Abstract—A boundary-discontinuous double Fourier series method for obtaining analytical solutions to the problems of deformation of finite moderately thick cross-ply doubled-curved panels, with four different boundary constraints, is presented in Part I of this investigation. In this segment, the equations that arise by way of satisfying these boundary conditions, thereby ensuring well-posedness of the formulation and existence of the solutions thus obtained, are presented first. The convergence characteristics of the series solutions, especially their dependence on laminations and boundary constraints, are then numerically investigated in detail. Other numerical results presented here include (i) verification/comparison with the available FSDT (first-order shear deformation theory)- and CLT (classical lamination theory)-based analytical solutions, (ii) investigation of the effects of length-to-thickness and radius-to-length ratios on the response of antisymmetric and symmetric cross-ply doubly-curved panels, with various boundary constraints, and (iii) spatial variation of displacements, rotations and moments.

1. INTRODUCTION

In the accompanying Part I of this study (Chaudhuri and Kabir, 1993), a methodology, which exploits a recently published (Chaudhuri, I1989) novel double Fourier series approach, to solve the boundary-value problem of deformation of moderately thick cross-ply doubly-curved panels of rectangular planform, subjected to transverse loads was presented. Sets of $5mn+2m+2n$ linear algebraic equations in terms of $5mn+8m+8n+4$, $5mn+8m+8n+4$, $5mn+6m+6n$ and $5mn+6m+6n$ unknown coefficients for the cases of SS1, SS2, SS4 and C4 [following the classification of Hoff and Rehfield (1965)] boundary conditions, have been obtained from the governing system of five highly coupled linear partial differential equations (PDEs), that arise from using first-order shear deformation theory (FSDT) and Sanders' kinematic relations. The details of the equations obtained from the boundary conditions, which are presented in this part, are not discussed there in addition to the relevant numerical results.

The convergence characteristics of displacements, rotations and moments, and their dependence on lamination and boundary constraint are investigated in detail. In addition to the study of the sensitivity of the response of moderately thick cross-ply spherical panels to laminations and boundary constraints, numerical results presented include (i) comparison with the available FSDT- and CLT-based analytical solutions, (ii) study of the effects of (a) thickness and (b) curvature on displacements and moments, and (iii) spatial variation of these response quantities. The equations, appendices and references of Part I of this paper are referred to by their original numbers, years, etc., preceded by I, e.g. (I6) denotes eqns (6) of Part I.

2. BOUNDARY CONDITIONS

SS1 boundary condition

For this boundary condition, the governing system of PDEs (I6)–(I8) provide, in total, $5mn+2m+2n$ equations in $5mn+8m+8n+4$ unknowns. The remaining $6m+6n+4$

† Current address: EMRC, Troy, MI 48083, U.S.A.

equations, necessary to match the number of unknowns, are obtained by way of satisfying the prescribed boundary conditions. The geometric boundary conditions are automatically satisfied by the assumed displacement functions (I11). With regard to the natural boundary conditions, substitution of the appropriate derivatives [e.g. eqns (I13)–(I15) and (A1)] into eqns (I12a) and equating the coefficients of $\sin(\alpha_m x_1)$, $\sin(\beta n x_2)$, etc., result in the following linear algebraic equations:

(i) $N_1(0, x_2) = N_1(a, x_2) = 0$:

$$B_{11}(i_n \pm j_n) + A_{11}(c_n \pm d_n) - A_{12}\beta_n(e_n \pm f_n) = 0, \tag{1a}$$

(ii) $N_2(x_1, 0) = N_2(x_1, b) = 0$:

$$B_{22}(k_m \pm l_m) - A_{12}\alpha_m(a_m \pm b_m) + A_{22}(g_m \pm h_m) = 0, \tag{1b}$$

(iii) $N_6(0, x_2) = N_6(a, x_2) = 0$:

$$\begin{aligned}(A_{66} - cB_{66})\left[\frac{1}{2}(\beta_n U_{0n} + \gamma_n a_0 + \psi_n b_0) + \sum_{m=1}^{\infty}(\pm 1)^m(\beta_n U_{mn} + \gamma_n a_m + \psi_n b_m)\right] \\ + (A_{66} + cB_{66})\left[\frac{1}{2}e_n + \sum_{m=1}^{\infty}(\pm 1)^m(\alpha_m V_{mn} + \gamma_m e_n + \psi_m f_n)\right] \\ + B_{66}\left[\beta_n X_{0n} + \sum_{m=1}^{\infty}(\pm 1)^m(\beta_n X_{mn} + \alpha_m Y_{mn})\right] = 0,\end{aligned} \tag{1c}$$

$$\begin{aligned}(A_{66} - cB_{66})\left[\frac{1}{4}a_0 + \frac{1}{2}\sum_{m=1}^{\infty}(\pm 1)^m a_m\right] + (A_{66} + cB_{66})\left[\frac{1}{4}e_0 + \frac{1}{2}\sum_{m=1}^{\infty}(\pm 1)^m(\alpha_m V_{m0}\right. \\ \left. + \gamma_m e_0 + \psi_m f_0)\right] + B_{66}\sum_{m=1}^{\infty}(\pm 1)^m \alpha_m Y_{m0} = 0,\end{aligned} \tag{1d}$$

(iv) $N_6(x_1, 0) = N_6(x_1, b) = 0$:

$$\begin{aligned}(A_{66} - cB_{66})\left[\frac{1}{2}a_m + \sum_{n=1}^{\infty}(\pm 1)^n(\beta_n U_{mn} + \gamma_n a_m + \psi_n b_m)\right] \\ + (A_{66} + cB_{66})\left[\frac{1}{2}(\alpha_m V_{m0} + \gamma_m e_0 + \psi_m f_0) + \sum_{n=1}^{\infty}(\pm 1)^n(\alpha_m V_{mn} + \gamma_m e_n + \psi_m f_n)\right] \\ + B_{66}\left[\sum_{n=1}^{\infty}(\pm 1)^n(\beta_n X_{mn} + \alpha_m Y_{mn}) + \alpha_m Y_{m0}\right] = 0,\end{aligned} \tag{1e}$$

$$\begin{aligned}(A_{66} - cB_{66})\left[\frac{1}{4}a_0 + \frac{1}{2}\sum_{n=1}^{\infty}(\pm 1)^n(\beta_n U_{0n} + \gamma_n a_0 + \psi_n b_0)\right] \\ + (A_{66} + cB_{66})\left[\frac{1}{4}e_0 + \frac{1}{2}\sum_{n=1}^{\infty}(\pm 1)^n e_n\right] + B_{66}\sum_{n=1}^{\infty}(\pm 1)^n \beta_n X_{0n} = 0,\end{aligned} \tag{1f}$$

(v) $M_1(0, x_2) = M_1(a, x_2) = 0$:

$$D_{11}(i_n \pm j_n) + B_{11}(c_n \pm d_n) - B_{12}\beta_n(e_n \pm f_n) = 0, \tag{1g}$$

(vi) $M_2(x_1, 0) = M_2(x_1, b) = 0$:

$$D_{22}(k_m \pm l_m) - B_{12}\alpha_m(a_m \pm b_m) + B_{22}(g_m \pm h_m) = 0. \tag{1h}$$

In eqns (1), the "+" sign applies for the first of the two conditions, i.e. for the edges x_1 or $x_2 = 0$, while the "−" sign represents the conditions at the edges $x_1 = a$ or $x_2 = b$.

SS2 boundary condition

With regard to the geometric boundary conditions [see eqns (I10b)], whenever any of the assumed functions, given by eqns (I11), fails to automatically satisfy a prescribed geometric boundary condition, the delinquent solution function is forced to satisfy it. In this particular case, $u_1 = 0$ at the edges, $x_1 = 0, a$, and $u_2 = 0$ at the edges $x_2 = 0, b$ yield $2m+2n$ additional equations, which can be written as follows:

$$\sum_{m=1}^{\infty} \psi_m U_{mn} = 0, \quad U_{0n} + \sum_{m=1}^{\infty} \gamma_m U_{mn} = 0, \quad \text{for } n = 1, 2, \ldots, \tag{2a}$$

$$\sum_{n=1}^{\infty} \psi_n V_{mn} = 0, \quad V_{m0} + \sum_{n=1}^{\infty} \gamma_n V_{mn} = 0, \quad \text{for } m = 1, 2, \ldots. \tag{2b}$$

The remaining equations that arise from the natural boundary conditions (N_6 and M_1 or $M_2 = 0$), prescribed at the appropriate edges, are similar to their SS1 counterparts and are omitted in the interest of brevity of presentation.

SS4 boundary condition

In this case, the geometric boundary conditions, u_1 or $u_2 = 0$ and the natural boundary conditions, M_1 or $M_2 = 0$, applied at the appropriate edges, supply equations, similar to their SS2 counterparts.

C4 boundary conditions

The geometric boundary conditions supply $4m+4n$ equations (from satisfying $u_1 = 0$ at the edges $x_1 = 0, a$ and $u_2 = 0$ at the edges $x_2 = 0, b$), identical to eqns (2) for the SS2 case, while the conditions, $\phi_1 = 0$ at the edges $x_1 = 0, a$, and $\phi_2 = 0$ at the edges $x_2 = 0, b$, supply the following linear algebraic equations:

$$\sum_{m=1}^{\infty} \psi_m X_{mn} = 0, \quad X_{0n} + \sum_{m=1}^{\infty} \gamma_m X_{mn}, \quad \text{for } n = 1, 2, \ldots, \tag{3a}$$

$$\sum_{n=1}^{\infty} \psi_n Y_{mn} = 0, \quad Y_{m0} + \sum_{n=1}^{\infty} \gamma_n Y_{mn}, \quad \text{for } m = 1, 2, \ldots. \tag{3b}$$

3. SOLUTION TECHNIQUE OF SIMULTANEOUS EQUATIONS

In the interest of computational efficiency, the $5mn+2m+2n$ linear algebraic equations [e.g. eqns (I17) for the case of SS1 boundary condition], resulting from the governing PDEs, are first solved for U_{mn}, V_{mn}, W_{mn}, X_{mn} and Y_{mn} in terms of constant coefficients a_n, b_n, etc., following the procedure laid down by Chaudhuri (I1989). These are then substituted in the linear algebraic equations generated from the boundary conditions [e.g. eqns (2) for the case of SS1 boundary condition]. This operation reduces the size of the problems under consideration by one or more orders of magnitude, finally resulting in $6m+6n+4$, $6m+6n+4$, $4m+4n$ and $4m+4n$ linear algebraic equations for the SS1, SS2, SS4 and C4 boundary conditions, respectively.

4. RESULTS AND DISCUSSIONS

For illustrative purposes, numerical results for antisymmetric (0°/90°), and symmetric (0°/90°/0°) cross-ply spherical panels of square planform, and subjected to uniformly

Table 1. Comparison of FSDT- and CLT- computed normalized deflections of an antisymmetric (0°/90°) cross-ply flat panel (material type 2)

Transverse displacement, u_3^*		
CLT Whitney (I1970)	FSDT Kabir and Chaudhuri (1991)	FSDT (Present, $R = 10^8$)
2.861	2.860	2.845

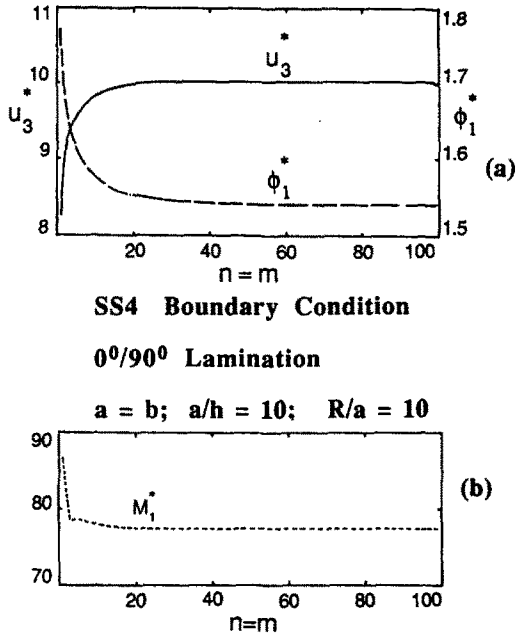

Fig. 1. Convergence of (a) u_3^*, ϕ_1^*, and (b) M_1^* of a square moderately-thick ($a/h = 10$) and moderately-deep ($R/a = 10$) antisymmetric cross-ply (0°/90°) spherical panel, with SS4 boundary condition.

distributed transverse loads, are presented. The following material properties are assumed:

(a) Material type I (Pagano and Hatfield, 1972)—used in Figs 1–15 and Tables 2, 3: $E_1 = 175.78$ GPa (25,000 Ksi),

$$E_1/E_2 = 25, \quad G_{12}/E_2 = G_{13}/E_2 = 0.5, \quad G_{23}/E_2 = 0.2, \quad \nu_{12} = 0.25.$$

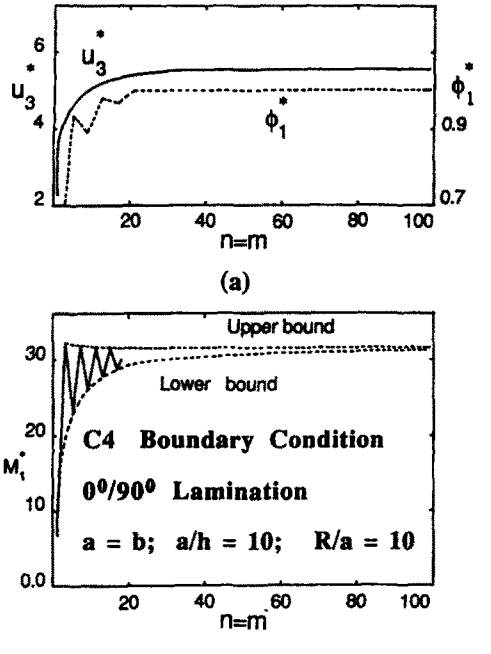

Fig. 2. Convergence of (a) u_3^*, ϕ_1^*, and (b) M_1^* of a square moderately-thick ($a/h = 10$) and moderately-deep ($R/a = 10$) antisymmetric cross-ply (0°/90°) spherical panel, with C4 boundary condition.

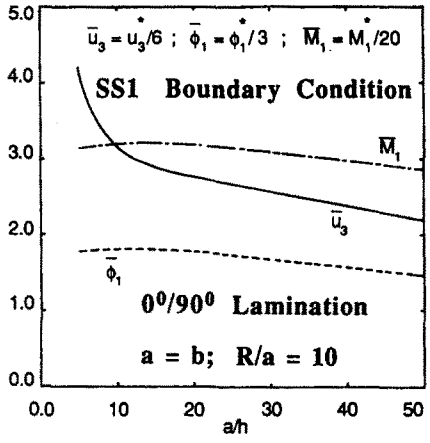

Fig. 3. Variation of the normalized central displacement, rotation ($x_1 = 0$, $x_2 = a/2$), and central moment of square moderately-deep ($R/a = 10$) antisymmetric cross-ply (0°/90°) spherical panels with SS1 boundary condition, with a/h ratio.

(b) Material type II (Whitney, I1970)—used in Table 1 : $E_1 = 281.2$ GPa (40,000 Ksi),

$$E_1/E_2 = 40, \quad G_{12}/E_2 = G_{13}/E_2 = 1.0, \quad G_{23}/E_2 = 0.2, \quad \nu_{12} = 0.25,$$

in which E_1 and E_2 are the surface-parallel Young's moduli in x_1 and x_2 coordinate directions, respectively, while G_{12} denotes surface-parallel shear modulus. G_{13} and G_{23} are transverse shear moduli in the x_1–x_3 and x_2–x_3 planes, respectively, while ν_{12} is major Poisson's ratio on the x_1–x_2 surface. The shear correction factors, $K_1^2 = K_2^2 = 5/6$, are assumed in the absence of better information [see, e.g., Bert and Chen (1978)]. This is because of the difficulty encountered in measurement of the transverse shear moduli in a lamina. Additionally, manufacturing defects, such as local fiber waviness regions and associated resin-rich areas that can trigger kink band type shear failure, when subjected to shear or compression loading [see Chaudhuri (1991) for details], play a significant role in

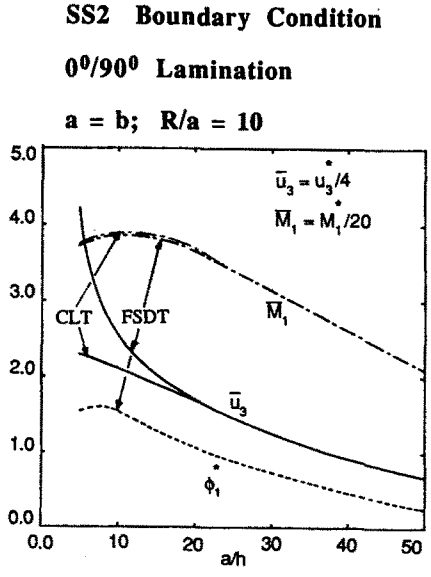

Fig. 4. Variation of the normalized central displacement, rotation ($x_1 = 0$, $x_2 = a/2$), and central moment of square moderately-deep ($R/a = 10$) antisymmetric cross-ply (0°/90°) spherical panels with SS2 boundary condition, with a/h ratio.

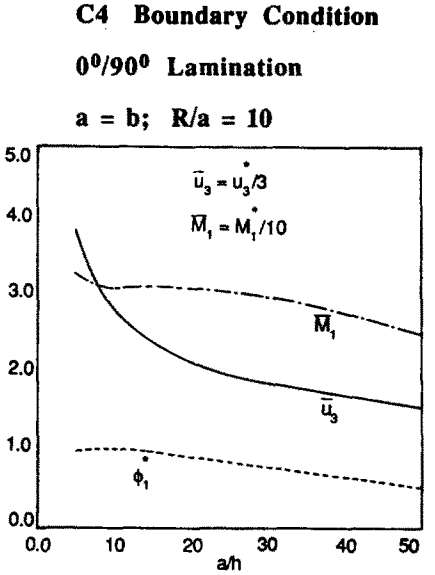

Fig. 5. Variation of the normalized central displacement, rotation ($x_1 = a/4$, $x_2 = a/2$), and central moment of square moderately-deep ($R/a = 10$) antisymmetric cross-ply (0°/90°) spherical panels with C4 boundary condition, with a/h ratio.

the deformation behavior of real-life composite laminates. All the numerical results with the single exception of comparison with CLT-based solution (Table 1) due to Whitney (I1970), are computed using the material type I. The following non-dimensionalized quantities are defined:

$$u_3^* = \frac{10^3 E_2 h^3}{qa^4} u_3, \quad M_1^* = \frac{10^3}{qa^2} M_1, \quad \phi_1^* = \frac{10^2 E_2 h^3}{qa^3} \phi_1,$$

in which a represents the curved span length of a side of the spherical panel and is assumed equal to 812.8 mm (32 in.), while h is its total thickness. q denotes the uniformly distributed

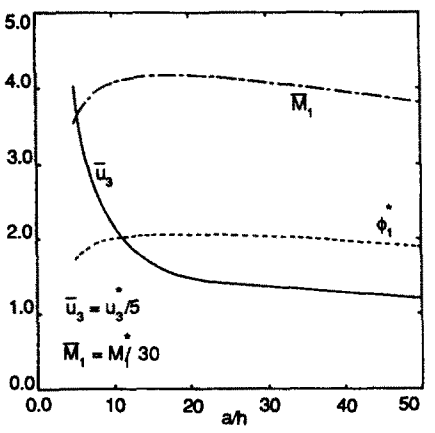

Fig. 6. Variation of the normalized central displacement, rotation ($x_1 = 0$, $x_2 = a/2$), and central moment of square moderately-deep ($R/a = 10$) symmetric cross-ply (0°/90°/0°) spherical panels with SS1 boundary condition, with a/h ratio.

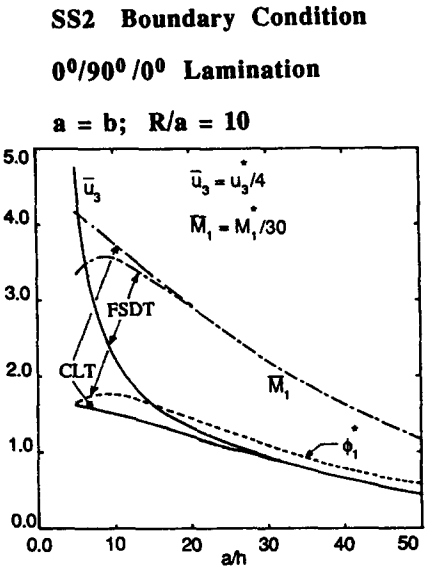

Fig. 7. Variation of the normalized central displacement, rotation ($x_1 = 0$, $x_2 = a/2$), and central moment of square moderately-deep ($R/a = 10$) symmetric cross-ply (0°/90°/0°) spherical panels with SS2 boundary condition, with a/h ratio and comparison with the CLT counterparts.

transverse load. For all the numerical results presented in Figs 1–11, the displacement, u_3, and moment, M_1, are computed at the center of the panel, while the rotation, ϕ_1, is computed at the points $(0, b/2)$ and $(a/4, b/2)$ for the simply-supported, and clamped boundary conditions, respectively.

Figure 1(a) displays the convergence (with $m = n$) of non-dimensionalized transverse displacement, u_3^* and rotation, ϕ_1^*, of moderately thick ($a/h = 10$) antisymmetric cross-ply (0°/90°) spherical panels, with the SS4-type simply-supported boundary condition, prescribed at all four edges. Rapid and monotonic convergence is observed. The magnitudes of u_3^* and ϕ_1^*, computed using $m = n = 27$ are within 0.899% and 0.389%, respectively, of the corresponding "converged" results ($m = n = 78$). Although the convergence plot of the central moment, M_1^*, presented in Fig. 1(b) exhibits an initial lack of monotonicity for $m = n \leqslant 5$, a rapid and monotonic convergence follows thereafter. For example, M_1^*, computed using $m = n = 27$, is within 0.202% of the corresponding "converged" result at

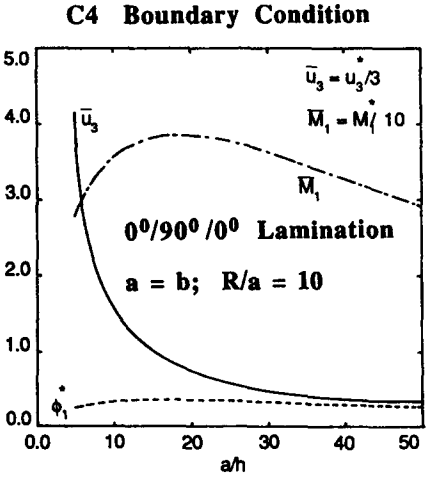

Fig. 8. Variation of the normalized central displacement, rotation ($x_1 = a/4$, $x_2 = a/2$), and central moment of square moderately-deep ($R/a = 10$) symmetric cross-ply (0°/90°/0°) spherical panels with C4 boundary condition, with a/h ratio.

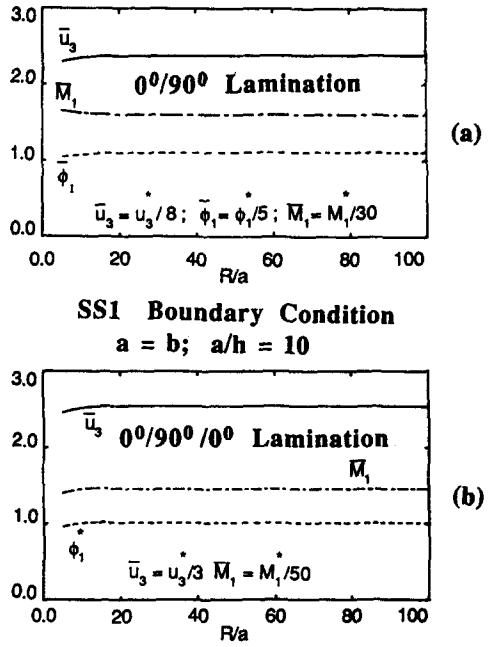

Fig. 9. Variation of the normalized central displacement, rotation ($x_1 = 0$, $x_2 = a/2$), and central moment of square moderately-thick ($a/h = 10$) (a) antisymmetric (0°/90°) and (b) symmetric (0°/90°/0°) cross-ply spherical panels with SS1 boundary condition, with R/a ratio.

$m = n = 78$. Convergence of u_3^*, ϕ_1^* and M_1^* of moderately thick symmetric cross-ply (0°/90°/0°) panels of otherwise the same geometry and with the same boundary conditions as above, tends to be faster compared to their antisymmetric (0°/90°) counterparts. Additionally, u_3^* and M_1^* vs $m = n$ plots exhibit initial nonmonotonicity. Since the con-

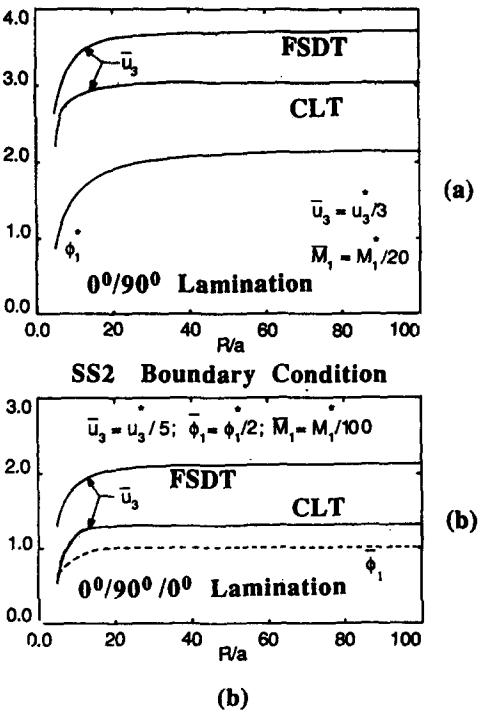

Fig. 10. Variation of the normalized central displacement, and rotation ($x_1 = 0, x_2 = a/2$), of square moderately-thick ($a/h = 10$) (a) antisymmetric (0°/90°) and (b) symmetric (0°/90°/0°) cross-ply spherical panels with SS2 boundary condition, with R/a ratio and comparison with the CLT counterparts.

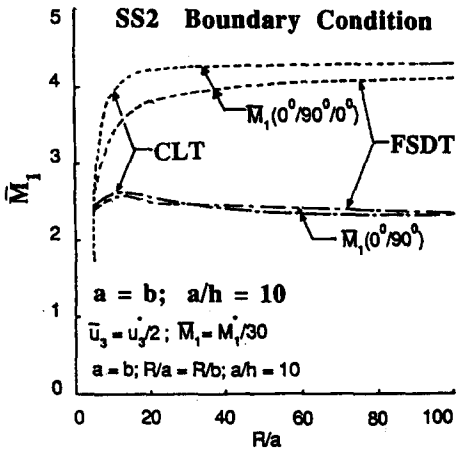

Fig. 11. Variation of the normalized central moment of square moderately-thick ($a/h = 10$) antisymmetric (0°/90°) and symmetric (0°/90°/0°) cross-ply spherical panels with SS2 boundary condition, with R/a ratio and comparison with the CLT counterparts.

vergence characteristics of both types of laminates are otherwise similar, these plots are not presented here in the interest of brevity.

FSDT-based convergence plots of an antisymmetric cross-ply spherical panel, with the SS2 boundary condition (not shown), are numerically too close to their SS4 counterparts to warrant a separate plotting. This is because both the conditions prescribe $u_n = 0$ (instead of $N_n = 0$) at a boundary—a choice that appears to have a major influence on the response of antisymmetric cross-ply panels under uniform loads. Likewise, the convergence characteristics of the response quantities for antisymmetric cross-ply panels, with SS1 and SS3 boundary conditions (not shown in the interest of brevity of presentation), where $N_n = 0$, instead of $u_n = 0$, is prescribed at a boundary, are numerically very close.

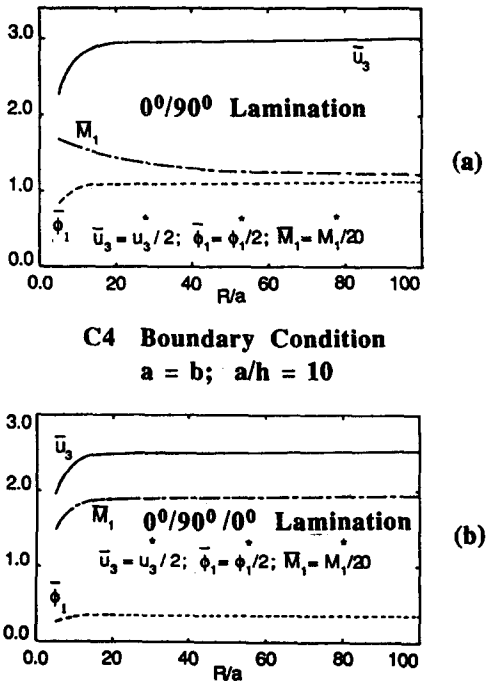

Fig. 12. Variation of the normalized central displacement, rotation ($x_1 = a/4$, $x_2 = a/2$), and central moment of square moderately-thick ($a/h = 10$) (a) antisymmetric (0°/90°) and (b) symmetric (0°/90°/0°) cross-ply spherical panels with C4 boundary condition, with R/a ratio.

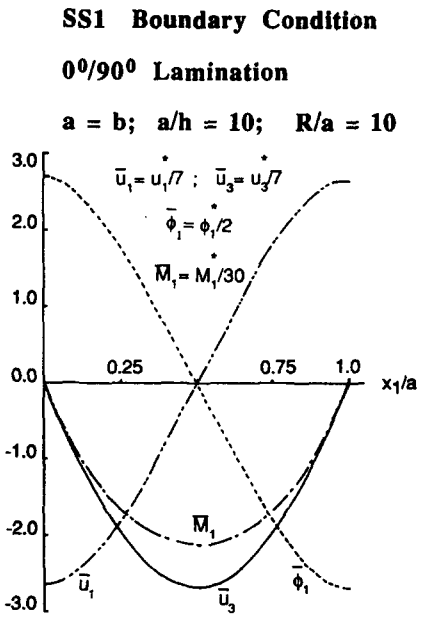

Fig. 13. Variation of normalized displacements, rotation and moment along the center line, $x_2 = a/2$, of a square moderately-thick ($a/h = 10$) and moderately-deep ($R/a = 10$) antisymmetric cross-ply (0°/90°) spherical panel with SS1 boundary condition.

The convergence of u_3^* of a moderately thick ($a/h = 10$) antisymmetric cross-ply (0°/90°) panel, with the C4-type clamped boundary condition, shown in Fig. 2(a), is similar, in nature, to its SS4 counterpart, while the corresponding σ_1^*, computed at the point ($a/4, b/2$) and shown in Fig. 2(a), unlike its SS4 counterpart, oscillates noticeably for $m = n \leqslant 21$. Oscillations for $m = n > 21$ can be regarded as negligible—for example, the difference in results computed at $m = n = 29$ and 31 is only 0.148%. However, a bounded oscillation, with upper and lower bounds shown by dashed lines in Fig. 2(b), is observed for the central moment M_1^*. For the case of ϕ_1^* and M_1^*, the sum of the Fourier series tends to converge

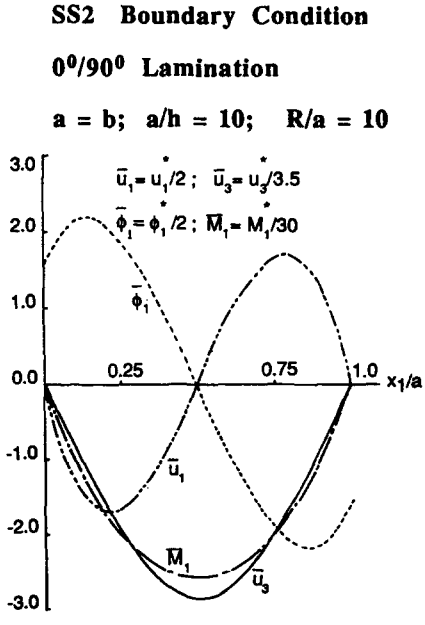

Fig. 14. Variation of normalized displacements, rotation and moment along the center line, $x_2 = a/2$, of a square moderately-thick ($a/h = 10$) and moderately-deep ($R/a = 10$) antisymmetric cross-ply (0°/90°) spherical panel with SS2 boundary condition.

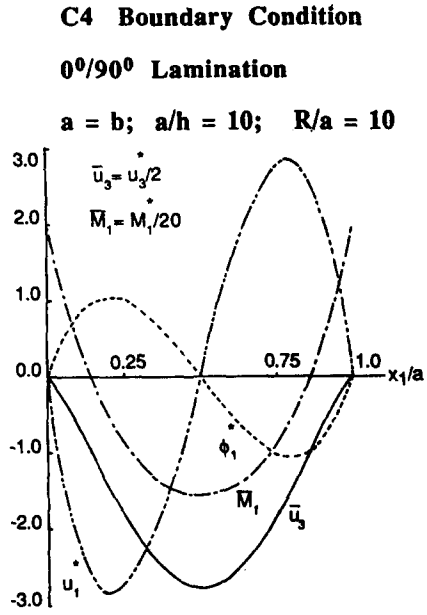

Fig. 15. Variation of normalized displacements, rotation and moment along the center line, $x_2 = a/2$, of a square moderately-thick ($a/h = 10$) and moderately-deep ($R/a = 10$) antisymmetric cross-ply (0°/90°) C4-type clamped spherical panel.

to the average value of upper and lower bounds for sufficiently large m, n, which is in accord with the theory of Fourier series, as expounded by Hobson (I1926). For example, the error in $M\dagger$, defined to be {average of lower ($m = n = 97$) and upper bound ($m = n = 99$)—average of lower ($m = n = 51$) and upper bound ($m = n = 53$)}/{average of lower ($m = n = 97$) and upper bound ($m = n = 99$)}, is approximately 0.627%. The converged normalized central deflection of a thin ($a/h = 100$) antisymmetric (0°/90°) cross-ply plate obtained from the present solution, computed using $R = 10^8$ and material type II, reduces to its flat laminate counterpart [see Chaudhuri and Kabir (1992)], and also compares favorably (approximately 0.56% difference—see Table 1) with Whitney's (I1970) CLT-based boundary-discontinuous solution and FSDT-based boundary continuous displacement solution due to Kabir and Chaudhuri (1991).

Table 2 presents a comparison of the central deflections, u_3^*, rotations, $\phi\dagger$ and central moments, $M\dagger$, of antisymmetric (0°/90°) cross-ply panels, with SS1, SS2, SS3, SS4 and C4 boundary conditions, prescribed at all four edges. The numerical results for the case of SS1 and SS2 are evaluated using $m = n = 78$, while for the case of SS3, SS4 and C4, $m = n = 99$ is used. The present results for the C4 boundary condition are numerically indistinguishable from their counterparts, obtained by Kabir and Chaudhuri (in review), using a generalized

Table 2. Comparison of computed normalized displacements, rotations and moments of square moderately-thick ($a/h = 10$) and moderately-deep ($R/a = 10$) antisymmetric (0°/90°) cross-ply spherical panels for various boundary conditions

Boundary conditions	u_3^*	$\phi\dagger$	$M\dagger$	$m = n$
SS1	18.83	5.410	64.14	78
SS2	10.10	1.539	77.52	78
SS3†	18.66	5.352	64.41	99
SS4	10.11	1.540	77.53	99
C4	5.58	1.030	31.70	99

† Computed using Navier solution.

Table 3. Comparison of computed normalized displacements, rotations and moments of square moderately-thick ($a/h = 10$) and moderately-deep ($R/a = 10$) symmetric (0°/90°/0°) cross-ply spherical panels for various boundary conditions

Boundary conditions	u_3^*	ϕ_1^*	M_1^*	$m = n$
SS1	10.53	2.006	122.55	78
SS2	9.17	1.750	106.78	78
SS3†	10.47	1.996	121.92	99
SS4	9.17	1.750	106.79	99
C4	4.73	0.322	35.89	99

† Computed using Navier solution.

Navier's approach, where the boundary conditions are satisfied *a priori*. This validates the applicability of the present method in the case of the C4-type clamped boundary condition. The numerical results for the SS3 boundary condition, computed using Navier's approach, are very close to their SS1 counterparts. A similar agreement is also observed between the results for the SS2 and SS4 boundary conditions. Computed u_3^* for the SS2 and SS4 boundary conditions appear to be numerically closer to their C4 counterparts, as compared to their SS1 and SS3 counterparts. Similar agreements between SS1 and SS3, and SS2 and SS4 results are also observed for the case of symmetric (0°/90°/0°) laminates (Table 3). However, computed u_3^* results for the SS2 and SS4 boundary conditions are closer to their SS1 and SS3 counterparts than to their C4 counterpart.

In what follows, numerical results will be restricted to SS1-, SS2-type simply-supported and C4-type clamped boundary conditions. SS3 and SS4 results are generally too close to their SS1 and SS2 counterparts to warrant separate meaningful plottings. Figures 3–5 and 6–8 present variations, with respect to a/h ratio, of u_3^*, ϕ_1^*, and M_1^* of moderately deep (relatively shallow) ($R/a = 10$) antisymmetric (0°/90°) and symmetric (0°/90°/0°) cross-ply panels, respectively, with SS1, SS2 and C4 boundary conditions, prescribed at the edges. Sensitivity of the response quantities of interest to thickness, lamination and boundary constraint is self-evident in these plots. For example, displacements, rotations and moments, for the case of the SS2 boundary condition, display more pronounced variations than their SS1 and C4 counterparts. Figures 4 and 7 show comparison of the FSDT-based central deflections and moments, of antisymmetric and symmetric spherical panels, respectively, subjected to the SS2 boundary condition, with their CLT-based counterparts [Chaudhuri and Kabir (in review)] over a wide range of the a/h ratios. These plots exhibit the effect of transverse shear deformation on the computed deflection, captured by the FSDT (and neglected by the CLT), especially in the thick shell regime, for both types of lamination. Detailed discussions on this issue are available in Chaudhuri and Kabir (in review) and will be omitted here in the interest of brevity of presentation. Furthermore, as expected [see Chaudhuri and Seide (1987) and Seide and Chaudhuri (1987)], the thickness effect, especially in the case of thicker panels ($a/h \leqslant 20$), is more pronounced in the computed normalized transverse displacements than in the corresponding rotations and moments. It is further noteworthy, that a more pronounced thickness effect is observed in the computed displacement, edge rotation (which applies to the simply-supported boundary conditions only) and central moment of symmetric (0°/90°/0°) panels, as compared to their antisymmetric (0°/90°) counterparts. There is reason to believe [see Abu-Arja and Chaudhuri (1989)] that the effect of thickness is compensated by the bending–stretching coupling effect, a characteristic of antisymmetric and unsymmetric laminates.

Variations of u_3^*, ϕ_1^* and M_1^*, with respect to R/a ratio, of moderately thick ($a/h = 10$) antisymmetric (0°/90°) and symmetric (0°/90°/0°) cross-ply panels, are presented in Figs 9(a, b), 10(a, b), 11 and 12(a, b), for the SS1, SS2 and C4 boundary conditions, respectively. Sensitivity of the response quantities of interest to the curvature, lamination and boundary

constraint is self-evident in these plots. For example, variations of transverse displacements, rotations and moments of both antisymmetric (0°/90°) and symmetric (0°/90°/0°) cross-ply panels, with SS1 boundary condition, shown in Figs 9(a, b), respectively, are not that prominent for $R/a > 10$. The same is not true, however, for the case of the SS2 boundary condition [Figs 10(a, b), 11], where the membrane effect is quite pronounced, even for relatively shallow panels ($R/a > 10$). For the case of antisymmetric (0°/90°) cross-ply panels, the moment $M\dagger$ decreases monotonically with the increase of R/a ratio [Fig. 10a)], while $M\dagger$ of symmetric (0°/90°/0°) laminates shows a completely different behavior [Fig. 10(b)]. Figures 10(a, b) and (11) also present comparisons of the present FSDT-based normalized central deflection, u_3^*, and moment, M^*, respectively, of antisymmetric (0°/90°) and symmetric (0°/90°/0°) cross-ply moderately thick ($a/h = 10$) spherical panels, subjected to the SS2 boundary condition, with their CLT-based counterparts. As expected, the CLT underpredicts the deflection, while overpredicting the moment in the case of symmetric laminates, over the entire range of R/a ratios. Detailed discussions on the subject are available in Chaudhuri and Kabir (in review) and are, therefore, excluded here in the interest of brevity of presentation. Numerical results for variations, with respect to the ratio R/a, of u_3^* and $\phi\dagger$ of both antisymmetric (0°/90°) and symmetric (0°/90°/0°) cross-ply panels, with the C4 boundary condition, presented in Figs 12(a, b), respectively, show similar behavior, whereas the plot for $M\dagger$ vs R/a ratio is different in the two cases. M^*, of antisymmetric (0°/90°) cross-ply panels, increases with R/a ratio, while exhibiting a contrasting behavior in the case of their symmetric (0°/90°/0°) counterparts. It is noteworthy that the membrane action due to the effect of curvature has a complex interaction with the bending–stretching type coupling effect, caused by the asymmetry of lamination. This interaction is most pronounced in the case of prescribed simply-supported boundary conditions with constraint, $u_n = 0$ [e.g. SS2 boundary condition, Figs 10(a, b), 11], and least prominent in the case of prescribed simply-supported boundary constraint, $N_n = 0$ [e.g. SS1 boundary condition, Figs 9(a, b)].

Variations of $u\dagger$, u_3^*, $\phi\dagger$ and M^*, of moderately thick ($a/h = 10$) and moderately deep ($R/a = 10$) antisymmetric (0°/90°) panels with SS1, SS2 and C4 boundary conditions, along the centerline, $x_2 = a/2$, are shown in Figs 13–15, respectively. In all these plots, transverse displacement, u_3^*, assumes its maximum magnitude at the center of the panel, where the surface-parallel displacement, $u\dagger$ and rotation, $\phi\dagger$ vanish. For the case of SS1 boundary condition (Fig. 13), $u\dagger$ and $\phi\dagger$ attain their maxima at the appropriate edges (i.e. at $x_1 = 0$ and a). The rotation, $\phi\dagger$, for the case of SS2 and C4 boundary conditions, reaches its maximum magnitudes near the one-quarter and three-quarter points (Figs 14 and 15). A similar trend is also observed in the case of $u\dagger$ as shown in Figs 14 and 15, respectively, for SS2 and C4 boundary conditions.

5. CONCLUSIONS

The key conclusions that emerge from the numerical results on cross-ply spherical panels, presented in this paper, can be summarized as follows:

(i) The effect of the transverse shear deformation is compensated to a certain extent by the bending–stretching coupling effect—a characteristic of unsymmetric laminates.

(ii) Antisymmetric cross-ply spherical panels, by virtue of the bending–stretching coupling effect, are more sensitive to the boundary condition of surface-parallel displacement normal to an edge, $u_n = 0$, than the corresponding rotational condition, $\phi_n = 0$. Numerical results clearly demonstrate that the SS1 and SS3 results are virtually indistinguishable and the same is true for the SS2 and SS4 conditions. More importantly, the SS2/SS4 results for transverse displacement are numerically closer to the corresponding clamped, C4, results than to their SS1/SS3 counterparts.

(iii) The deformation behavior of symmetric cross-ply spherical panels more closely resembles homogeneous orthotropic ones (e.g. unidirectional composite shells), compared to their antisymmetric counterparts, because all four simply-supported boundary conditions yield relatively close results.

(iv) The membrane action due to the effect of curvature has a complex interaction with the bending–stretching type coupling effect, caused by the asymmetry of lamination. This interaction is most pronounced in the case of prescribed simply-supported boundary conditions with constraint, $u_n = 0$ (e.g. SS2/SS4 boundary conditions), and least prominent in the case of prescribed simply-supported boundary constraint, $N_n = 0$ (e.g. SS1/SS3 boundary conditions).

The numerical results presented herein extend our understanding of the complex deformation behavior of finite-dimensional moderately-thick cross-ply doubly-curved panels, and should serve as baseline solutions for future comparisons with such approximate numerical techniques as finite element and finite difference, in the context of FSDT.

Acknowledgements—The authors wish to acknowledge the useful comments of the reviewers on an earlier version of the manuscript. They also wish to thank the editor, Professor Steele, for his kind advice and encouragement in the preparation of the revised manuscript.

REFERENCES

Abu-Arja, K. R. and Chaudhuri, R. A. (1989). Influence of transverse shear deformation on scaling of cross-ply cylindrical shells. *J. Compos. Mater.* **23,** 673–694.

Bert, C. W. and Chen, T. L. C. (1978). Effect of shear deformation on vibration of antisymmetric angle-ply laminated rectangular plates. *Int. J. Solids Structures* **14,** 465–473.

Chaudhuri, R. A. (1991). Prediction of the compressive strength of thick-section advanced composite laminates. *J. Compos. Mater.* **25,** 1244–1276.

Chaudhuri, R. A. and Kabir, H. R. H. (1992). Influence of lamination and boundary constraint on the deformation of moderately thick cross-ply rectangular plates. *J. Compos. Mater.* **26,** 51–77.

Chaudhuri, R. A. and Kabir, H. R. H. (1993). Sensitivity of the response of moderately thick cross-ply doubly-curved panels to lamination and boundary constraint—I. Theory. *Int. J. Solids Structures* **30**(2), 263–272.

Chaudhuri, R. A. and Kabir, H. R. H. (in review). Static and dynamic Fourier analysis of finite general cross-ply doubly-curved panels using classical shallow shell theories.

Chaudhuri, R. A. and Seide, P. (1987). Triangular finite element for analysis of thick laminated plates. *Int. J. Num. Meth. Engng* **24,** 1203–1224.

Kabir, H. R. H. and Chaudhuri, R. A. (1991). A generalized Navier's solution of clamped moderately thick cross-ply plates. *Compos. Struct.* **17,** 351–366.

Kabir, H. R. H. and Chaudhuri, R. A. (in review). On boundary continuous displacement static and dynamic Fourier analysis of arbitrarily laminated clamped doubly-curved panels.

Pagano, N. J. and Hatfield, S. J. (1972). Elastic behavior of multilayered bidirectional composites. *AIAA Jl* **10,** 931–933.

Seide, P. and Chaudhuri, R. A. (1987). Triangular finite element for analysis of thick laminated shells. *Int. J. Num. Meth. Engng* **24,** 1563–1579.

APPENDIX

Certain displacement functions and their derivatives, at the boundaries, may be expressed in terms of the boundary-discontinuous Fourier coefficients. For example:

$$u_1(x_1, 0) = -\frac{b}{4}\sum_{m=0}^{\infty}(a_m + b_m)\cos(\alpha_m x_1), \tag{A1a}$$

$$u_1(x_1, b) = \frac{b}{4}\sum_{m=0}^{\infty}(a_m - b_m)\cos(\alpha_m x_2). \tag{A1b}$$

$u_{1,1}(0, x_2)$, $u_{1,1}(a, x_2)$; $u_2(0, x_2)$, $u_2(a, x_2)$; $u_{2,2}(x_2, 0)$, $u_{2,2}(x_2, b)$; $\phi_{1,1}(0, x_2)$, $\phi_{1,1}(a, x_2)$ and $\phi_{2,2}(x_2, 0)$, $\phi_{2,2}(x_2, b)$ can similarly be defined in terms of c_n, d_n; e_n, f_n; g_m, h_m; i_n, j_n and k_m, l_m, respectively.